Modelling of Water Transport through Mixed-Ion Conducting Dense Ceramics

Selgin Al,[1]*† Feng Song[2] and Guangru Zhang[3]‡

1. Department of Chemical Engineering and Advanced Materials, Newcastle University, NE1 7RU Newcastle upon Tyne, UK
2. College of Chemical Engineering, Shandong University of Technology, Zibo 255049 Shandong Province, China
3. Department of Chemical Engineering and Advanced Materials, Newcastle University, NE1 7RU Newcastle upon Tyne, UK

This study develops and demonstrates a model that characterizes defect transports, responsible for water transport within dense ceramics, and calculates the diffusion coefficients for those defects. The multi-species mass transfer processes within yttrium doped barium cerates are modelled by applying the Nernst-Planck equation to the system. The Nernst-Planck equation with suitable boundary conditions is adopted to compute defect diffusion coefficients in COMSOL Multiphysics. All related equations, based on charge and defect conservation, are solved numerically and validated experimentally. The model also predicts the concentration distribution of the defects and potential profiles throughout the membranes. The results provided convenient insights about the water transport and charge distribution as a function of membrane thickness.

Keywords: yttrium doped barium cerates, water transport, perovskite ceramics

INTRODUCTION

Ceramic based protonic conductors such as yttrium-doped barium cerate or zirconate, from the ABO_3 perovskite family, exhibit dual ion conductivity (proton and oxide ion) at intermediate temperatures. The proton conduction discovery in these types of perovskite materials[1] resulted in shifting from high-temperature oxide ion conductors to intermediate temperature proton conductors. These types of ceramic membranes have been envisioned to be used for various applications such as sensors, gas separation membranes, fuel cells, and electrolysers.[2,3] Thus, a great deal of research has been focused on improving their properties such as conductivity, chemical, and thermodynamic stability by co-doping with different elements, combining with different oxides (e.g. barium zirconates), or using sintering additives (e.g. nickel, cobalt oxides) in order to use them as steam electrolysers, hydrogen pumps, and electrolyte membranes.[4] Depending on the gaseous environment, these materials are capable of transporting multiple species such as protons, oxide ions, and water simultaneously. This makes them leading candidates especially for solid oxide fuel cells operating at intermediate temperatures. It is known that yttrium-doped barium cerate can effectively transport water[5,6] (hydration and dehydration) which relies on diffusion of protonic defect $\left(OH_O^{\bullet}\right)$ and oxygen vacancy $\left(V_O^{\bullet\bullet}\right)$ through the membrane. There have been various studies carried out to understand transport of water through these membranes[3,5,7] and determine diffusion coefficients of protonic defect and oxygen vacancy via thermogravimetric analysis (TGA),[7,8] conductivity measurements,[9,10] and dilatometry analysis.[5,11]

In the present work we propose and develop a model for the first time in order to compute the diffusion coefficients for protonic defect and oxygen vacancy transport within the BCY10 ($BaCe_{0.9}Y_{0.1}O_{3-\delta}$) and BCY20 ($BaCe_{0.8}Y_{0.2}O_{3-\delta}$) ceramic membranes as well as their concentration gradients. The flux of protonic defect and oxygen vacancy in a dense solid membrane is affected by concentration and electrical potential gradient. The internal electrical potential is established to maintain electro neutrality within the membrane. The transport process of defects through the membrane can be expressed and simulated via the Nernst-Planck equation. The Nernst-Planck equation considers both concentration and electrical potential gradient for their transport within a membrane and can be solved computationally. The Nernst-Planck equation with suitable boundary conditions has been adopted to compute diffusion coefficients in COMSOL Multiphysics. The model has also been validated with experimental results. The model provides an accurate calculation of the concentration distribution of defects and electrical potential changes throughout the membranes.

MODEL DEVELOPMENT

Physical Model

Figure 1 demonstrates the schematic representation of the physical hydration process of BCY membranes. The model allows modelling membrane surface hydration and simulating the change in electrical potential and diffusions of protonic defects and oxygen vacancies ($OH_O^{\bullet}$, $V_O^{\bullet\bullet}$) within the BCY membranes. The transport of charged species inside the membrane is directly related to the molecular species (such as water vapour, oxygen etc.) in the gas phase compositions. Therefore, electronic defects (electrons and holes) inside the BCY membranes have not been

†Current address: S. Al, Department of Physics, Faculty of Arts and Sciences, Ahi Evran University, Kirsehir, Turkey
‡Current address: G. Zhang, State Key Laboratory of Materials-Oriented Chemical Engineering, Nanjing Tech University, Nanjing, 210009, P.R. China
* *Author to whom correspondence may be addressed.*
E-mail: selgin.al@ahievran.edu.tr
Can. J. Chem. Eng. 96:1637–1644, 2018

DOI 10.1002/cjce.23098
Published online 5 December 2017 in Wiley Online Library (wileyonlinelibrary.com).

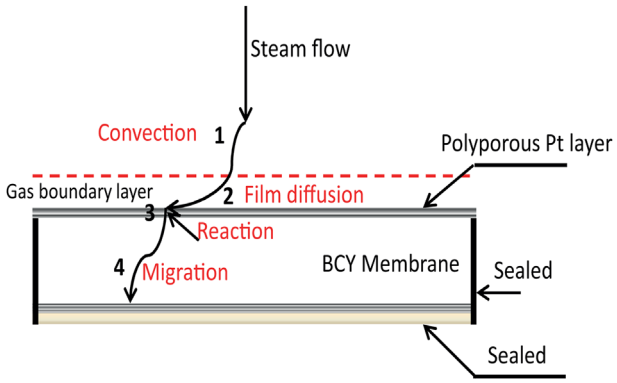

Figure 1. Schematic representation of steps of the membrane hydration.

taken into account, since the probability of their existence is low as the surrounding gas in this study is composed of 1 % H_2O in N_2. As a result, the oxygen partial pressure is taken to be very low and constant. The model adopted the Nernst-Planck equation with solution boundary conditions at the interface of the membrane and gases.

The transportation of water is composed of four steps as sketched in Figure 1 which are:

1. Convection of water vapour (steam) in the gas phase.
2. Diffusion of water through the boundary layer and platinum layer.
3. Water disassociation and incorporation on the membrane surface.
4. Protonic defect and oxygen vacancy migration inside the membrane.

Mathematical Model

This part of the model comprises three bodies: governing equations, initial values, and boundary conditions. The mathematical implementations for the four physical steps above have been detailed and are explained as follows.

1. The transport phenomenon is not affected by the convection (water vapour) in the gas, therefore, it can be ignored. The water partial pressure hence is taken to be constant on the exposed side of the membrane boundary layer.
2. The driving force equation for water diffusion in the boundary layer can be expressed as:

$$\frac{dC_{S,H_2O}(t)}{dt} = -k_f \times \left(C^*_{H_2O}(t) - C_{out}\right) - R_{e,H_2O} \tag{1}$$

where k_f is the H_2O mass transfer coefficient, m/s; C_{S,H_2O} is the surface concentration of H_2O, mol/m^2; R_{e,H_2O} is surface reaction rate of H_2O with the membrane, mol/(m$^2 \cdot$ s); $C^*_{H_2O}(t)$ is the water equilibrium concentration with the protonic defect concentration on the membrane surface, mol/m^3; and C_{out} is the bulk concentration, mol/m^3. Equation (1) represents the water concentration on the membrane surface which is time dependent and requires initial values. The initial values considered (based on experimental conditions) are: $C_{out} = P_{out}/RT$, $P_{out} = 0.01$ atm, $t = 0, C_{S,H_2O}(L,t) = 0$.

3. The third step involves the water reaction with the membrane surface; the corresponding equation can be presented as:

$$H_2O + V_O^{\bullet\bullet} + O_O^x \overset{K}{\leftrightarrow} 2OH_O^{\bullet} \tag{2}$$

$$K = \frac{k_1}{k_2} = \frac{C^2_{OH_O^{\bullet}}}{C_{V_O^{\bullet\bullet}} C_{O_O^x} P^*_{H_2O}/P_0} \tag{3}$$

The reactants' concentrations will be deducted by the forward reaction, on the other hand they will be increased by the reverse reaction, and therefore the net reaction rate of Equation (3) is expressed as follows:

$$R_a = \left(k_1\ C_{V_O^{\bullet\bullet}}\ C_{O_O^x} P^*_{H_2O}/P_0\right) - k_2 C^2_{OH_O^{\bullet}} \tag{4}$$

$$R_a = k_1 \left\{ \left(C_{V_O^{\bullet\bullet}}\ C_{O_O^x}\ P^*_{H_2O}/P_0\right) - \frac{1}{K} C^2_{OH_O^{\bullet}} \right\} \tag{5}$$

where K is the reaction equilibrium constant; k_1 is the forward reaction rate constant, m^2/mol $\cdot$ s; k_2 is the reverse reaction rate constant, m^2/mol $\cdot$ s; $P^*_{H_2O}$ is the water partial pressure on the membrane surface, Pa; R_a is the reaction rate of Equation (3), mol/m$^2 \cdot$ s; and P_0 is the atmospheric pressure, Pa.

The reactants and products reaction rates can be depicted with Equations (6) to (9), respectively.

$$R_{e,H_2O} = -R_a \tag{6}$$

$$R_{e,O_O^x} = -R_a \tag{7}$$

$$R_{e,V_O^{\bullet\bullet}} = -R_a \tag{8}$$

$$R_{e,OH_O^{\bullet}} = 2R_a \tag{9}$$

where R_e is species reaction rate on the membrane surface. Reaction rates from Equation (6) to (9) are time dependent and initial values are necessary. The species initial values in the membranes utilized in the current work are computed from the stoichiometry of membrane equilibrium with the given gas-phase composition at the surface and given in Table 1. The yttrium doping concentrations taken into account in the analysis are 20 mol% for BCY20 and 10 mol% for BCY10.

4. The diffusion of two species ($OH_O^{\bullet}$ and $V_O^{\bullet\bullet}$) inside the BCY membranes can be expressed by the Nernst-Planck equation. The Nernst-Planck equation is a mass conservation equation that defines the impact of an ionic concentration gradient and an electric field on the chemical species migration is given as:[12]

$$\frac{\partial c_i}{\partial t} = -\frac{\partial J_i}{\partial x} \tag{10}$$

$$\frac{\partial c_i}{\partial t} = c_i u - D_i \nabla c_i - c_i U_i z_i e \nabla V \tag{11}$$

The convection term ($c_i u$) accommodates background velocity u (m/s) and c_i concentration of species i (mol/m^3). The diffusion term ($D_i \nabla c_i$) is only presented by the diffusion coefficient D_i (m^2/s). The migration term ($c_i U_i z_i e \nabla V$) accommodates mobility of ions U (velocity per unit applied force m/Ns), z_i (charge number of species), e (elementary charge of an electron, C), and electrical potential (V).

Table 1. Species initial concentrations

Species	Concentration	Charge
BCY20 ($BaCe_{0.8}Y_{0.2}O_{2.9}$)	1.7371×10^4 mol/m^3	0
O_O^x	5.0377×10^4 mol/m^3	0
Y'_{Ce}	3.4743×10^3 mol/m^3	-1
$V_O^{\bullet\bullet}$	1.7371×10^3 mol/m^3	2
$OH_O^{\bullet}$	0	1
Species	**Concentration**	**Charge**
BCY10 ($BaCe_{0.9}Y_{0.1}O_{2.95}$)	1.5130×10^4 mol/m^3	0
O_O^x	4.4633×10^4 mol/m^3	0
Y'_{Ce}	1.513×10^3 mol/m^3	-1
$V_O^{\bullet\bullet}$	7.565×10^2 mol/m^3	2
$OH_O^{\bullet}$	0	1

Substituting U_i from the Nernst-Einstein relation (which relates mobility of species to diffusion coefficients) and using Faraday ($F = eN_A$) and Boltzmann constants ($k_B = R/N$) U_i can be written as:

$$U_i = \frac{D_i}{k_B T} = \frac{FD_i}{RTe} \tag{12}$$

The Nernst-Planck equation can now be expressed as:

$$\frac{\partial c_i}{\partial t} = c_i u - D_i \nabla c_i - c_i z_i \frac{D_i F}{RT} \nabla V \tag{13}$$

This study considers one-dimensional transport through the membranes along the thickness. The convection part in the equation can be neglected since the convection rate in the gas phase is too fast as compared to diffusion processes. Thus Equation (13) can be written as:

$$J_i = -D_i \frac{dc_i}{dx} - c_i z_i \frac{D_i F}{RT} \frac{dV_i}{dx} \tag{14}$$

The mass conservation equation for one-dimensional transport of ions through the membranes is expressed as:

$$\frac{dc_i}{dt} + \frac{dJ_i}{dx} + c_i u = R_i \tag{15}$$

By substituting Equation (14) into Equation (15), the equation can be written as:

$$\frac{dc_i}{dt} + \frac{d}{dx}\left(-D_i \frac{dc_i}{dx} - c_i z_i \frac{D_i F}{RT} \frac{dV_i}{dx}\right) = R_i \tag{16}$$

Equation (16) can be adopted for all the species inside the BCY membrane and presents the basic form of a series of equations utilized to determine the parameters along the thickness of the membrane.

The electro neutrality condition is employed throughout the membrane:

$$\sum_i z_i C_i = 0 \tag{17}$$

The net charge all over the membrane is zero. There are two movable charges inside the BCY membrane which are $OH_O^{\bullet}$ and $V_O^{\bullet\bullet}$ and both are positive. Hence, a negative charge must be considered for the electro neutrality condition. The negative charge taken into account is Y'_{Ce} which is immovable since it is a part of the rigid crystal lattice. Thus the diffusion coefficient is taken as zero.

The electrical potential is computed by adding all of the charged species mass transfer equations and multiplying this sum with Fz_i (Equation (18)).

The current density relation (related to defect concentration) can be written as:

$$I_t = F\sum_{i=1}^{n} z_i \left(-D_i \frac{dc_i}{dx} - c_i z_i \frac{D_i F}{RT} \frac{dV_i}{dx}\right) \tag{18}$$

Equation (18) depicts electric charge conservation which associates electric potential with concentration. The initial values and boundary conditions are defined below for Equations (16) and (18). These equations are sufficient to simulate the concentration distribution of ions, vacancies, and the electric potential inside the membrane as a function of time and space.

Discretization of the Membrane

The diffusion of water inside the membrane is treated as one-dimensional transport to calculate defect distribution throughout the membrane. This assumption can be used only when membrane thicknesses are small compared to radial surface areas. Therefore, diffusion is adopted to occur in only one direction. The isolated surface electrical potential at x = L is specified as 0 V. The membrane can be discretized into finite volumes as displayed in Figure 2.

When solely the diffusion is considered, based upon mass balance, the specie (i) concentration with time can be expressed as in Equation (19) where S is the surface area, m^2.

$$S \times [C_i(x, t+\Delta t) - C_i(x,t)] \times \Delta x = S \times [J_i(x,t) - J_i(x+\Delta x, t)] \times \Delta t \tag{19}$$

Boundary Conditions

The dissociation of water happens on the BCY membrane surface. $OH_O^{\bullet}$ is generated on this surface and permeates inside the BCY

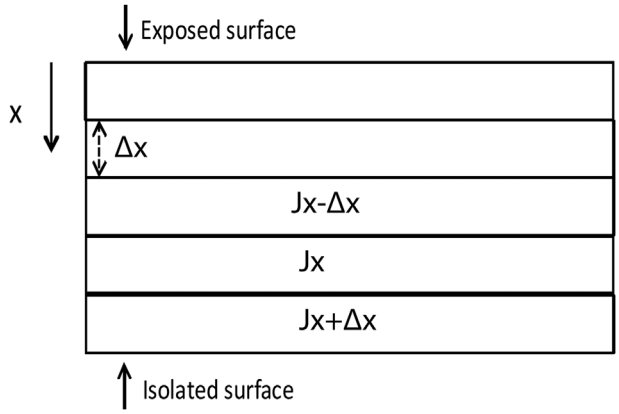

Figure 2. Visualisation of discretization of the membrane $J_{x-\Delta x}$ and $J_{x+\Delta x}$ represent neighbouring parts.

membrane (in the positive direction shown in Figure 1) where $J_{OH_o^\bullet}$ is the flux of $OH_O^\bullet$ at the boundary of membrane, mol/m^{2}s.

At the boundary, the mass balance of $OH_O^\bullet$ can be expressed as:

$$S \times \left(C_{OH_o^\bullet}(t+\Delta t)\right)|_{x=0} - C_{OH_o^\bullet}(t)|_{x=0} = S \times \Delta t \times J_{OH_o^\bullet}(t)|_{x=0} + S \times \Delta t \times R_{OH_o^\bullet}(t)|_{x=0} \quad (20)$$

where $J_{OH_o^\bullet}$ is the flux of $OH_O^\bullet$ at the boundary of membrane, mol/m^{2}s, and $R_{OH_o^\bullet}$ is the surface reaction rate of $OH_O^\bullet$, mol/m^{2}s.

Following the same steps for $V_O^{\bullet\bullet}$, the boundary conditions for $OH_O^\bullet$ and $V_O^{\bullet\bullet}$ for both surfaces are:

x = 0 exposed surface boundary conditions:

$$J_{OH_o^\bullet}(t)|_{x=0} = -\frac{dC_{OH_o^\bullet}(t)}{dt}|_{x=0} + 2R_a|_{x=0} \quad (21)$$

$$J_{V_o^{\bullet\bullet}}(t)|_{x=0} = -\frac{dC_{V_o^{\bullet\bullet}}(t)}{dt}|_{x=0} - R_a|_{x=0} \quad (22)$$

$$V = 0 \quad (23)$$

x = L isolated surface boundary conditions:

$$\frac{dC_i}{dx} = 0 \quad (24)$$

$$\frac{dV}{dx} = 0 \quad (25)$$

The functions taken into account in this model to regress initial values of $D_{V_o^{\bullet\bullet}}$ and $D_{OH_o^\bullet}$ are:[7]

$$D_{V_o^{\bullet\bullet}} = 1.10 \times 10^{-6} exp\left(\frac{-52083.55}{8.314 \times T}\right) m^2/s \quad (26)$$

$$D_{OH_o^\bullet} = 2.03 \times 10^{-6} exp\left(\frac{-68480.23}{8.314 \times T}\right) m^2/s \quad (27)$$

Equation (2)'s reaction equilibrium constant which relates species concentration, is computed as:[7]

$$K = \frac{exp(\Delta H - \Delta ST)}{RT} = \frac{exp(162200 - 166.7T)}{8.314T} \quad (28)$$

where T is temperature (K).

The initial concentration of ions and vacancies considered in the model are presented in Table 1. COMSOL Multiphysics is used to get the solutions of the partial differential equations. The partial differential equations are computed with the backward Euler method with the initial assumptions. The species concentrations are computed using the Nernst-Planck equation including boundary conditions. The least-square method $\left(error\ function = \sum_{n=1}^{N}\sum_{n=1}^{N}\left(V_{cal} - V_{exp}\right)^2\right)$ is applied for regression of parameters.

EXPERIMENTAL

The BCY20 powder obtained from Marion Technology (France) was utilized to fabricate a BCY20 membrane. The solid state method was employed in order to prepare BCY10 powder. The precursors were: $BaCO_3$ (99 %, Aldrich), CeO_2 (99 %, Aldrich), and Y_2O_3 (99 %, Aldrich). The raw materials were blended in an appropriate ratio and ground in ethanol, the ball milling process was followed for 4 h, and then the mix was calcined at 1300 °C for 10 h. The fabrication of pellets were carried out by uniaxial pressing of 2 g of BCY powder at 3 tons using a 20 mm diameter die and then the pellets were sintered at 1450 °C for 12 h. X-ray diffraction (XRD) was employed to identify perovskite structure formation. The morphology of the membranes was examined by SEM. The final pellets were 1.44 mm thick for BCY20 and 1.14 mm thick for BCY10. An ESL Europe (type 5542-print grade) platinum resin was painted onto the membrane surfaces where they were exposed to water. A very small area of platinum (< 0.05 cm^2) was also employed in the middle of the membrane on the isolated side to obtain a good electrical connection with the membrane surface for measurements. Gold wires (Alfa Aesar) were used to make electrical connections. One of the membrane surfaces was isolated from the surroundings with a ceramic sealant and Sm-doped CeO_2 (SDC, which does not allow water to permeate) to obtain a hydrophobic surface. A sketch for the membrane setup is displayed in Figure 3.

An electrochemical workstation was used to carry out the potential measurements in a single reaction chamber at 700 °C and at atmospheric pressure. 1 % H_2O in N_2 (BOC, UK) was used during the hydration and He (BOC, UK) was used during the dehydration. The total flow rate of gas was 200 mL/min for both of them. Dry He was fed to the reaction chamber for 24 h in order to eliminate water content of the ceramic membrane before the experiments, and then the gas was switched to 1 % H_2O in N_2. A Grant Instrument water bath (Grant Scientific, UK) was used to control the water level. The inlet tubes were wrapped with heating tape so as to prevent water condensation in the lines during hydration. A moisture trap (Cole-Parmer CRS) was employed to assure that He does not include any water before entering the reaction chamber. The electrical potential changes of BCY membranes were verified by doing a blank experiment with an Al_2O_3 membrane under the same experimental conditions.

RESULTS AND DISCUSSION

Electrical Potential of Membranes

The changes in electrical potentials during hydration and dehydration processes for Al_2O_3, BCY20, and BCY10 are depicted

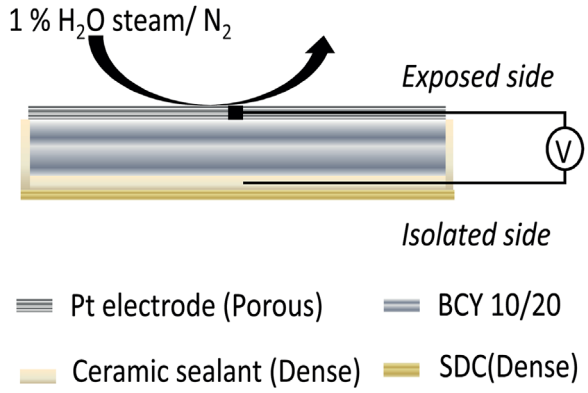

Figure 3. Schematics of membrane assembly to measure potential differences at 700 °C.

in Figure 4. Figure 4a represents the experiment result for the Al_2O_3 membrane which is exposed to the same experimental conditions as BCY membranes so as to verify potential changes of them owing to the hydration/dehydration process. The reason for choosing Al_2O_3 is that defect formation and the diffusion process do not occur within Al_2O_3 when it is exposed to a humid atmosphere.[13] Hydration and dehydration experiments are performed as follows: dry He is fed to the reaction chamber first and then that is switched to 1 % H_2O in N_2 at 500 s.

The blank experiment is done in the following order: firstly dry He is introduced to the reaction chamber and then it is switched to 1 % H_2O in N_2 at 500 s and kept the same until it is switched back to dry He again after 2500 s. Figure 4a shows that there is no change in potential with the change of surrounding atmosphere. Thus, the changes in potentials seen in Figure 4b and Figure 4c are associated with potential changes of BCY20 and BCY10 membranes during hydration and dehydration owing to formation and migration of charged species.

The calculated time to replace the atmosphere and ensure a steady water partial pressure inside the reaction chamber is short ($\sim$17 s) in comparison with potential equilibration time ($>$500 s). Thus, water partial pressure inside the chamber during hydration of the membranes can be taken as a constant parameter.

The potential change occurs within the membranes due to the concentration gradients of defects as the membranes hydrate or dehydrate. The membranes' electro neutrality is not affected by hydration. The driving force for water incorporation is the difference in water concentration between the atmosphere and membrane surfaces. In Figures 4b and 4c, the first peaks indicate the potential change when 1 % H_2O in N_2 enters into the reaction chamber and the second peaks imply when the feed gas is switched to dry He. As the water partial pressure increases, the ratio of protonic defects and oxygen vacancies changes immediately on the exposed side of the membrane. As the charged species diffuse within the membrane and concentrations become uniform again the potential difference disappears. For the aim of extracting diffusion coefficients of defects, the hydrations of the membranes process are enough, thus the discussions will continue based on hydration processes.

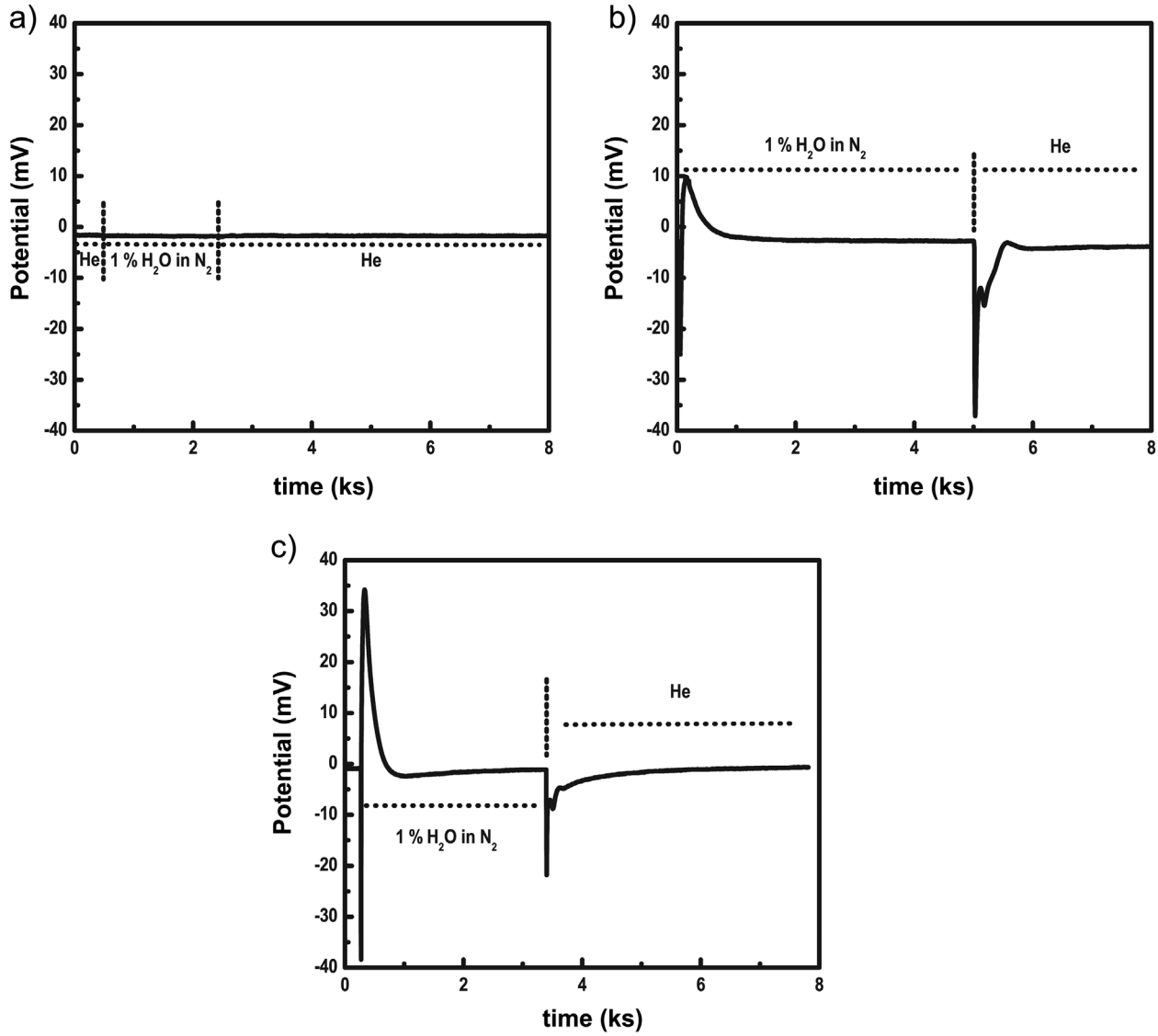

Figure 4. The potential changes of the membranes during hydration and dehydration measured under open circuit conditions at 700 °C. (a) Al_2O_3, (b) BCY20, (c) BCY10.

The difference in potential increases quickly and then decreases relatively slowly. This could indicate that surface reactions (adsorption, dissociation, incorporation) have fast kinetics. This kind of fast kinetics of hydration was observed by Schober and Coors.[5] A quick expansion was observed when ~0.03 % water was introduced to the dilatometer, followed by slow expansion. Moreover, protonic defects diffusion coefficients are found to be higher than oxygen vacancy diffusion coefficients.[14,15] The mass relaxation studies of $BaCe_{0.95}Yb_{0.05}O_{2.975}$ and $SrCe_{0.95}Yb_{0.05}O_{2.975}$ on hydration/dehydration showed quick diffusion of proton accompanied with sluggish diffusion of oxygen by Yoo et al.[16–18] Thus, it can be concluded that proton incorporation occurs fast into the membrane and diffuses fast by leaving oxide ions behind, which creates an unbalanced charge distribution within the membrane owing to the fixed negatively charged species distribution. When the oxide ion concentration becomes equal to that of the protons, the potential difference disappears. Figure 5 compares the experimental and model fit and depicts a good agreement between the model and experimental data ($R^2 = 0.997$ for BCY20 and $R^2 = 0.986$ for BCY10).

The time period (~100 s for BCY20 and ~75 s for BCY10, see Figure 5a and Figure 5b) and the magnitude of potential are different for the membranes (~13 mV for BCY20 and ~35 mV for BCY10). The reasons for this could be the difference in protonic defect concentration at the membrane surfaces, physical properties of membranes (e.g. thickness), and feed gas water concentration as suggested by Kee et al.[19] An increased water concentration from 1 % to 2 % in H_2 resulted in a potential change from 25 mV to 50 mV for 20 mol% yttrium-doped barium zirconate membrane (BZY20).[19] The potential profile for BZY20 was also predicted by Vøllestad et al.[20] using the Gauss law instead of electro neutrality conditions. 2 % water on the feed gas was used and a 20 mV potential difference was obtained with a two-chamber reactor (permeate side gas was inert). The values of potentials reported in this work are in the same order of magnitude as the previously reported data by Kee et al.[19] The potential profiles for different periods for the

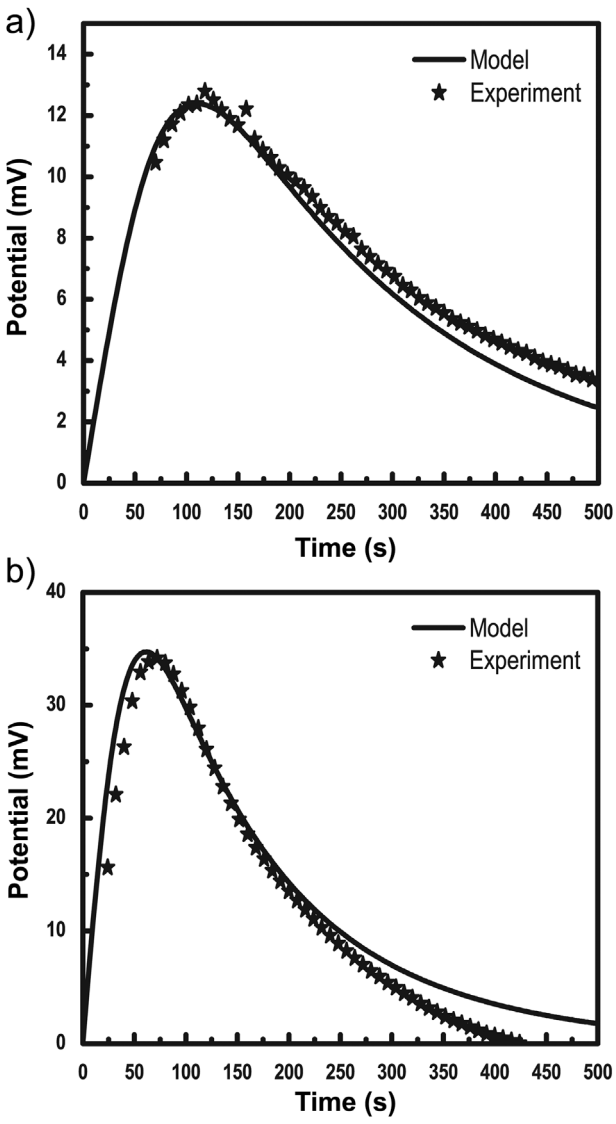

Figure 5. The comparisons of potential changes during hydration. Lines represent results from the model, stars represent results from the experiment. (a) BCY20, (b) BCY10.

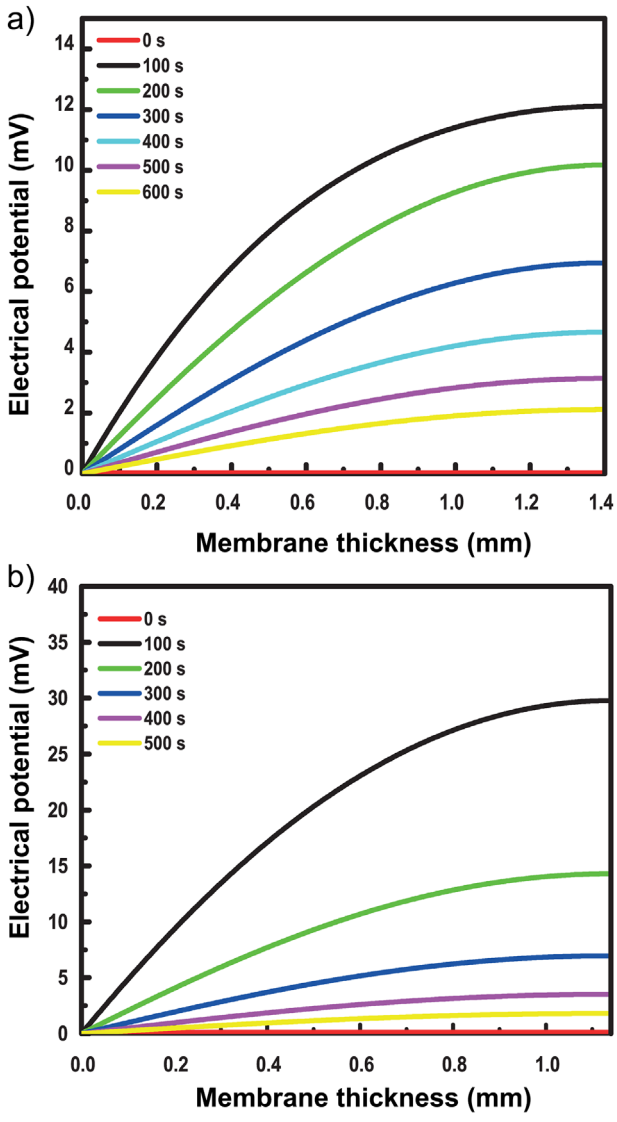

Figure 6. The profiles of potential differences during hydration for different periods within the membranes. (X = 0 represents "exposed side," x = L mm represents "isolated side," L = membrane thickness.) (a) BCY20, (b) BCY10.

Table 2. Diffusion coefficients obtained from the model

Parameter	BCY20 (cm^2/s)	BCY10 (cm^2/s)
$D_{V_o^{\bullet\bullet}}$	1.58×10^{-5}	1.27×10^{-5}
$D_{OH_o^{\bullet}}$	3.83×10^{-5}	6.2×10^{-5}

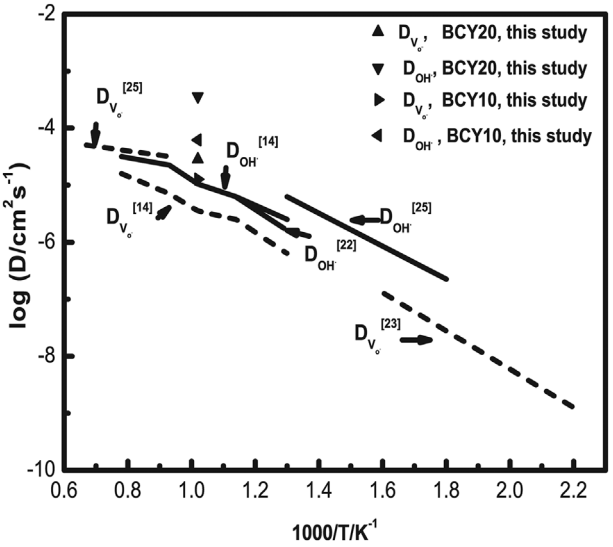

Figure 7. The diffusion coefficients comparisons with the literature.

hydration of membranes are presented in Figure 6 by using Equations (15) and (17). The potential difference changes rapidly for both membranes.

Diffusion Coefficients of Defects

The diffusion coefficients of defects are computed using the aforementioned model. The results are given in Table 2. The model takes into account the same initial values for both membranes from Kreuer et al.[7] The computation is done based on the Nernst-Planck equation with the boundary conditions. Protons have higher diffusion coefficients than oxygen vacancies for both membranes, which is in line with Oishi et al.[14] and Kreuer.[15] Kreuer et al.[7] determined protonic defect diffusion coefficients for BCY20 versus temperature from 50 °C to 350 °C and reported a rise from 10^{-10} to 10^{-8} cm^2/s as the temperature increases. On the other hand, the oxygen vacancy diffusion coefficient for BCY10 at 700 °C was obtained[21] as $D_{V_o^{\bullet\bullet}} = 5 \times 10^{-5} cm^2/s$ which is similar to the value obtained in this work.

The comparison of diffusion coefficients with literature is presented in Figure 7. The data in the literature is mostly determined by conductivity measurements.[14,21–23] However, most data in Figure 7 is for BCY10 since this material is commonly studied. Figure 7 shows a good agreement with literature within the accuracy of data; only a slight difference is seen in the values (Figure 7) which could be owing to grain boundaries. Diffusion of water was given as a fast process within grain boundaries.[24] On the other hand, conductivity is affected by grain boundaries negatively, thus the diffusion coefficients that are obtained from conductivity tend to be less. The studies on water diffusion on the grain boundaries are quite new[24] and hence, most data in Figure 7[14,22,23,25] did not consider this fact and it is highly possible that no correction was carried out. Therefore, an underestimation of diffusion coefficients is possible.

Concentration Distributions of Defects within the Membranes

The concentration profiles of defects upon hydration for different time periods are shown in Figure 8. This was obtained by solving the mass conservation equations in the model. There is a nonlinear distribution of defects along the membranes with time. As seen, the concentrations of protonic defects and oxygen vacancies have the opposite trend (asymmetric) for the membranes. This can be easily seen from the lines next to it. Oxygen vacancy concentration decreases while protonic defect concentration increases at the exposed surface which is in line with the model and hydration process of the membranes.

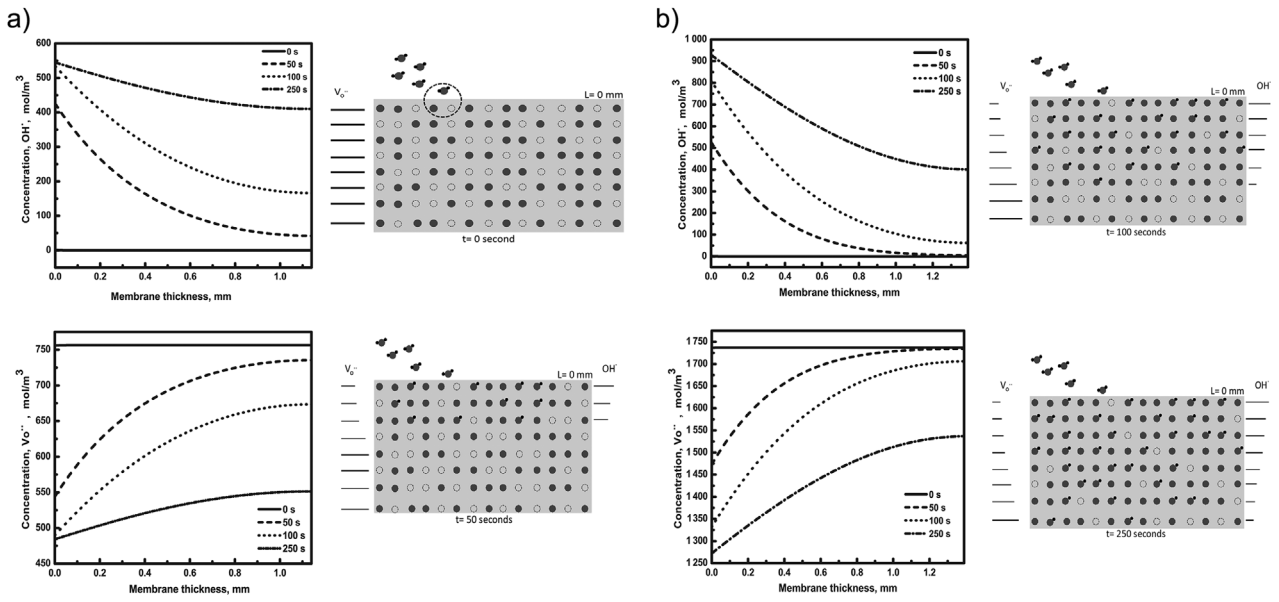

Figure 8. The concentration profiles of defects within the BCY membranes for different periods during hydration, (a) BCY10 and (b) BCY20, respectively. The right side schematics assist visualization of plots. The lines on the edges represent the changes in defect concentration. (•) represents protons, (◌) represents oxygen vacancy, (●) represents lattice oxygen, and (•) represents water.

Additionally, the variation in oxygen vacancy concentration profiles between surfaces and bulk is smaller compared to protonic defect concentration profiles. This could be the result of the stoichiometric ratios. Since the concentration of protonic defects rises rapidly at the exposed surface as water is introduced into the reaction chamber, it can be said that protonic defect formation is a fast process. The concentration versus time analysis also confirms this phenomenon. Figure 8 exhibits a fast increase in protonic defect concentration at the exposed surface at 50 s, followed by continuous increase with a slow rate. As the concentration gradients disappear with time, the membranes get hydrated fully. The concentration of protonic defects is higher for BCY20 than BCY10 at the exposed surface. This is due to BCY20 having higher oxygen vacancy availability.

CONCLUSION

An economical and direct model is developed in order to compute the diffusion coefficients and concentration distributions of defects within the membranes upon hydration. The model explains the steps of hydration of the membranes using the Nernst-Planck equation. The diffusion coefficients for protonic defects and oxygen vacancies for the BCY20 and BCY10 membranes are $D_{OH_O^\bullet} = 3.83 \times 10^{-5}\text{cm}^2/\text{s}$, $D_{V_O^{\bullet\bullet}} = 1.58 \times 10^{-5}\text{cm}^2/\text{s}$ and $D_{OH_O^\bullet} = 6.2 \times 10^{-5}\text{cm}^2/\text{s}$, and $D_{V_O^{\bullet\bullet}} = 1.27 \times 10^{-5}\text{cm}^2/\text{s}$, respectively. The results that are obtained are in agreement with the literature.

ACKNOWLEDGEMENTS

The authors would like to acknowledge the Ministry of National Education Turkey for funding. Also, we would like to thank Prof. Ian Metcalfe for the useful discussions and School of Chemical Engineering, Newcastle University, UK for the university's resources.

REFERENCES

[1] H. Iwahara, T. Esaka, H. Uchida, N. Maeda, *Solid State Ionics* **1981**, *3–4*, 359.

[2] T. Norby, *Solid State Ionics* **1999**, *125*, 1.

[3] W. G. Coors, *J. Power Sources* **2003**, *118*, 150.

[4] D. Medvedev, A. Murashkina, E. Pikalova, A. Demin, A. Podias, P. Tsiakaras, *Prog. Mater. Sci*. **2014**, *60*, 72.

[5] T. Schober, W. G. Coors, *Solid State Ionics* **2005**, *176*, 357.

[6] W. G. Coors, *J. Electrochem. Soc*. **2004**, *151*, A994.

[7] K. D. Kreuer, T. Dippel, Y. M. Baikov, J. Maier, *Solid State Ionics* **1996**, *86–88, Part 1*, 613.

[8] K. D. Kreuer, E. Schönherr, J. Maier, *Solid State Ionics* **1994**, *70–71, Part 1*, 278.

[9] W. Wang, A. V. Virkar, *J. Electrochem. Soc*. **2003**, *150*(1), A92.

[10] W. Grover Coors, R. Swartzlander, "Partial conductivity measurements in $BaCe_0.\ 9Y_0.\ _1O_{3\text{-}d}$ by impedance spectroscopy," *Proceedings of the 26th Risø International Symposium on Materials Science Solid State Electrochemistry*, Risø National Laboratory, Roskilde, 4–8 September **2005**, p. 185.

[11] T. Schober, J. Friedrich, D. Triefenbach, F. Tietz, *Solid State Ionics* **1997**, *100*, 173.

[12] J. H. Masliyah, S. Bhattacharjee, "Fundamental Transport Equations," in *Electrokinetic and Colloid Transport Phenomena*, John Wiley & Sons, Hoboken **2005**, p. 179.

[13] T. Shirai, H. Watanabe, M. Fuji, *Structural Properties and Surface Characteristics on Aluminum Oxide Powders*, Volume 9, Annual report of the Ceramics Research Laboratory, Nagoya Institute of Technology, Gokisocho **2009**, pp. 23–31, URL: http://id.nii.ac.jp/1476/00002232/.

[14] M. Oishi, S. Akoshima, K. Yashiro, K. Sato, J. Mizusaki, T. Kawada, *Solid State Ionics* **2008**, *179*, 2240.

[15] K. D. Kreuer, *Annu. Rev. Mater. Res*. **2003**, *33*, 333.

[16] H.-I. Yoo, J.-Y. Yoon, J.-S. Ha, C.-E. Lee, *Phys. Chem. Chem. Phys*. **2008**, *10*, 974.

[17] H.-I. Yoo, J. I. Yeon, J.-K. Kim, *Solid State Ionics* **2009**, *180*, 1443.

[18] H.-I. Yoo, C.-E. Lee, *Solid State Ionics* **2009**, *180*, 326.

[19] R. J. Kee, H. Zhu, B. W. Hildenbrand, E. Vøllestad, M. D. Sanders, R. P. O'Hayre, *J. Electrochem. Soc*. **2013**, *160*, F290.

[20] E. Vøllestad, H. Zhu, R. J. Kee, *J. Electrochem. Soc*. **2014**, *161*, F114.

[21] K. D. Kreuer, W. Munch, M. Ise, T. He, A. Fuchs, U. Traub, J. Maier, *Ber. Bunsen. Phys. Chem*. **1997**, *101*, 1344.

[22] A. Grimaud, J. M. Bassat, F. Mauvy, P. Simon, A. Canizares, B. Rousseau, M. Marrony, J. C. Grenier, *Solid State Ionics* **2011**, *191*, 24.

[23] K. D. Kreuer, *Solid State Ionics* **1999**, *125*, 285.

[24] K. B. Kostøl, A. Magrasó, T. Norby, *Int. J. Hydrogen Energ*. **2012**, *37*, 7970.

[25] K. D. Kreuer, *Solid State Ionics* **1997**, *97*, 1.

Manuscript received August 2, 2017; revised manuscript received September 30, 2017; accepted for publication October 27, 2017.